Nanoscale structural and mechanical characterization of thin bicontinuous cubic phase lipid films

Nanoscale structural and mechanical characterization of thin bicontinuous cubic phase lipid films

Andrea Ridolfi [a,b,c,], Ben Humphreys [d,e,f], Lucrezia Caselli [a,c], Costanza Montis [a,c], Tommy Nylander [d,e,f], Debora Berti [a,c], Marco Brucale [a,b,*] and Francesco Valle [a,b,*]*

a. Consorzio Interuniversitario per lo Sviluppo dei Sistemi a Grande Interfase, 50019 Firenze, Italy.

b. Consiglio Nazionale delle Ricerche, Istituto per lo Studio dei Materiali Nanostrutturati, 40129 Bologna, Italy.

c. Dipartimento di Chimica "Ugo Schiff", Università degli Studi di Firenze, 50019 Firenze, Italy.

d. Physical Chemistry, Department of Chemistry, Lund University, SE-221 00 Lund, Sweden.

e. Lund Institute of Advanced Neutron and X-ray Science - LINXS, SE- 223 70 Lund, Sweden.

f. NanoLund, Lund University, SE-221 00 Lund, Sweden.

** corresponding authors*

Statistical description

Number of words: 4280

Number of figures: 6

Abstract

The mechanical response of lipid membranes to nanoscale deformations is of fundamental importance for understanding how these interfaces behave in multiple biological processes; in particular, the nanoscale mechanics of non-lamellar membranes represents a largely unexplored research field. Among these mesophases, inverse bicontinuous cubic phase Q_{II} membranes have been found to spontaneously occur in stressed or virally infected cells and to play a role in fundamental processes, such as cell fusion and food digestion. We herein report on the fabrication of thin (~150 nm) supported Q_{II} cubic phase lipid films ($SQ_{II}Fs$) and on their characterization via multiple techniques including Small Angle X-Ray Scattering (SAXS), Ellipsometry and Atomic Force Microscopy (AFM). Moreover, we present the first nanomechanical characterization of a cubic phase lipid membrane, through AFM-based Force Spectroscopy (AFM-FS). Our analysis reveals that the mechanical response of these architectures is strictly related to their topology and structure. The observed properties are strikingly similar to those of macroscopic 3D printed cubic structures when subjected to compression tests in material science; suggesting that this behaviour depends on the 3D organisation, rather than on the length-scale of the architecture. We also show for the first time

that AFM-FS can be used for characterizing the structure of non-lamellar mesophases, obtaining lattice parameters in agreement with SAXS data. In contrast to classical rheological studies, which can only probe bulk cubic phase solutions, our AFM-FS analysis allows probing the response of cubic membranes to deformations occurring at length and force scales similar to those found in biological interactions.

Introduction

Lipid self-assembly encompasses a plethora of different mesophases, among which inverse bicontinuous cubic (Q_{II}) phases are some of the most intriguing[1–3]. These structures are characterized by a continuous lipid bilayer membrane that subdivides the three-dimensional space into two interwoven systems of water channels[4]. Curved membranes with structures similar to the lipid Q_{II} phases are believed to have an important role in Nature [5], which is not fully understood. These phases have been found to occur spontaneously in stressed or virally infected cells and are believed to be involved in numerous biological processes like cell fusion and food digestion[6]. Three types of lipid Q_{II} phase have been reported for lipid systems [3]: Q_{II}^{P}, Q_{II}^{D} and Q_{II}^{G}, respectively corresponding to the primitive (P), double diamond (D) and gyroid (G) infinite triply periodical minimal surfaces[7] (IPMS, see Figure S1 for their representation). In these mesophases, lipid molecules self-assemble in a curved bilayer, where the middle plane is described by one of the three above-mentioned minimal surfaces.

Compared to planar membranes, the complex structure of cubic phases imparts them with considerably higher membrane surface-to-volume ratios as well as a defined geometry with connected aqueous cavities [8]. Thanks to the amphiphilic nature of their lipid components, these characteristics can be exploited for the encapsulation of hydrophobic, hydrophilic and bioactive molecules, proteins and nanoparticles[9,10]. A considerable amount of effort has therefore been put into the study of cubic phases as protein crystallization scaffolds[11–13] and, more recently, as nanoparticle-based drug delivery systems (i.e. cubosomes)[8,14–17]. On the other hand, the development of homogenous supported lipid Q_{II} phase films has

received little attention despite their potential biomedical applications[18–21]. Analogously to how Supported Lipid Bilayers (SLBs)[22] are commonly used as surface-bound lamellar membrane models, Supported Q_{II} phase Films ($SQ_{II}Fs$) could be exploited as mimics of natural cubic membranes, allowing the study of their properties employing various surface techniques like Ellipsometry, Neutron/X-ray reflectivity and Atomic Force Microscopy (AFM). Results from such studies could help to shed light on biological interactions involving these intriguing and highly curved membranous interfaces. In this context, thin $SQ_{II}Fs$ approaching the typical length scales of naturally occurring cubic phase membranes[5] represent a versatile solution for advancing the current knowledge on the properties and functions of non-lamellar membranes.

To this purpose, we herein prepare thin (~150 nm**)** $SQ_{II}^{D}Fs$, starting from a glycerol-monooleate (GMO) solution. GMO is a natural food grade, biocompatible and biodegradable lipid, known to self-assemble into Q_{II} phases at standard temperature and pressures in excess water[23,24]. We then characterize the systems with multiple techniques including Small-Angle X-Ray Scattering (SAXS), Ellipsometry and AFM. Exploiting the surface-supported nature of $SQ_{II}^{D}Fs$, we also probe the lipid architecture by means of AFM-based Force Spectroscopy (AFM-FS). This allowed us to perform the first mechanical characterization of a bicontinuous cubic membrane at the nanoscale, showing that the mechanical response of these structures to a localized deformation is strictly related to their topology and geometry. Interestingly, our analysis shows that the nanomechanical behaviour observed in $SQ_{II}Fs$ closely resembles the one of macroscopic IPMS-inspired structures studied in material science[25–28], which possess desirable combinations of high impact resistance and low density. In contrast to classical rheological studies which can only probe the mechanical properties of Q_{II} bulk phases[29–31] , our AFM-FS analysis probes the response of these membranes to localized deformations, occurring at length and force scales approaching those found in biological and biomimetic interactions[32]. Moreover, the close relationship between the mechanical response and the topology of Q_{II}^{D} phase membranes allowed for the determination of their lattice parameter directly from the AFM force-distance curves, yielding results in good agreement with SAXS. According to our knowledge, this represents the first structural characterization of non-lamellar lipid

membranes through AFM-FS and provides an alternative solution to scattering and electron microscopy-based techniques. Through characterizing the structure and the mechanics of cubic phase membranes at the nanoscale, by means of perturbations that resemble the ones found in biological systems, our results could help to better rationalize the role and function of these not fully understood, yet biologically relevant self-assemblies.

Experimental

Glycerol Monooleate solution

Glycerol monooleate (mono- and diglycerides ratio 44:1 by weight), denoted as RYLO™ MG19 Glycerol Monooleate (GMO), was produced and provided by Danisco Ingredients (now Dupont, Brabrand, Denmark) with the following fatty acid composition (Lot No. 2119/65-1): 89.3 % oleic, 4.6% linoleic, 3.4% stearic and 2.7% palmitic acid. The product was then dissolved in chloroform reaching the desired concentrations for the different experiments.

Glycerol Monooleate bulk phases

In order to prepare the GMO bulk phase, the procedure employed by Mendozza et al. [33] was followed; briefly, 30 mg of GMO were solubilized in 1 mL of chloroform. The solvent was then removed with a gentle nitrogen flux, leaving a thin lipid film. The system was kept under vacuum overnight and sheltered from light. The dry film was fully hydrated with an excess of Milli-Q water and the sample was then centrifuged at least 5 times, changing the orientation of the vial (cap facing upward with another with cap facing downward) at each cycle. The lipid solution was then deposited on the thin Kapton film windows of the sandwich cells used for the SAXS measurements; the cells were subsequently filled with ultrapure water to ensure that the formed liquid crystalline is fully swollen in an excess of water.

Spin coating of Glycerol Monooleate films

GMO solutions were deposited on all substrates used in this study via spin coating. A single ≈10 µl drop was placed in the center of the substrate using a glass syringe. The substrate was then rotated at 2000 rpm for 35 seconds allowing the solvent to evaporate. Successful depositions resulted in

iridescent films uniformly covering the whole substrate. After spin coating, lipid films were hydrated (i.e., put into the fluid cells that were used in the various experiments) in order to let the lipid film equilibrate and self-assemble into the desired cubic architecture. Regarding monoolein hydrolysis, a previous study [34] showed that the content of free oleic acid for the type of sample used in the present work was below 1 mole percent after equilibrating with 5 wt% water at 40°C for 8 weeks. It is therefore unlikely that under the present conditions, 25 °C, and equilibration times of less than 1 day, there would be significant hydrolysis of the GMO to free oleic acid even though the lipid liquid crystalline phase are in excess of water. Ellipsometry measurements could not be performed either on Kapton substrates or on Highly Ordered Pyrolytic Graphite; the first substrate is not detectable by the polarized light while the surface of the second one is too rough for obtaining a clear signal from the reflected beam. To solve the issue, we relied on polystyrene, which is known to have a surface energy similar to the Kapton substrates. In order to obtain a Polystyrene layer that uniformly covers the entire Silicon surface, a 1% wt polystyrene solution in toluene was utilized. A 20 µl droplet was then added to the substrate while spinning it at 6000 rpm for 30 seconds. This procedure yielded a homogeneous polystyrene layer with thicknesses ranging from 15 to 20 nm. The thickness of the polystyrene layer was checked in every measurement by Ellipsometry, for our experiments the polystyrene layer average thickness was 16.1 ± 1.9 nm.

Small Angle X-ray Scattering

Small-angle X-ray scattering measurements were performed with a SAXS Lab Ganesha instrument (JJ-Xray, Denmark), equipped with a 30 W Cu X-ray micro-source (Xenocs, France) and a 2D 300 K Pilatus detector (Dectris, Switzerland). Measurements were performed with a pin-hole collimated beam with the detector positioned asymmetrically at a distance of 480 mm from the sample, to yield azimuthally averaged intensities as a function of the scattering vector (q) over the range 0.016 – 0.75 $Å^{-1}$. The magnitude of the scattering vector is defined by $q = (4\pi\sin\theta)/\lambda$, where λ equals to 1.54 Å, Cu Kα wavelength, and θ is half of the scattering angle. Samples were loaded in sandwich cells with thin Kapton film windows and placed in a thermostat stage at 25 °C, controlled using a Julabo T Controller CF41 (Julabo Labortechnik GmbH, Germany). The *d* spacing was obtained from the

positions of the Bragg peaks (q_{peak}) detected in the profiles of Figure 1 by using the following equation:

$$d=2\pi/q_{peak}$$

The lattice parameter of the cubic phase architecture, *a*, was calculated from the following equation:

$$a = d * (h^2 + k^2 + l^2)^{½}$$

where h, *k* and *l* are the Miller indexes that describe the crystalline planes of the lattice.

Spectroscopic Ellipsometry

Ellipsometry measures the change in polarization of light upon reflection from a surface or interface. The parameters that are used to characterize this polarization change are the amplitude ratio, Ψ, and the phase shift, Δ. Light reflection is described by the Fresnel reflection coefficients for the component of the light polarized parallel (p-polarization), r_P, and perpendicular (s-polarization), r_S, to the plane of incidence. The ratio r_P/r_S is related to the measured Ψ and Δ by the following equation:

$$r_P/r_S = tan(\Psi)e^{i\Delta}$$

When the film thickness increases to values on the same order of magnitude as the wavelength of the light, Δ and Ψ oscillate with the film thickness, making it challenging to be determined. To overcome this issue, spectroscopic ellipsometry offers the possibility to unambiguously determine the film thickness in the case of thicker films. Spectroscopic phase-modulated ellipsometer (SPME) (HORIBA Jobin Yvon, UVISEL) was therefore used for characterization of the interfacial films. The SPME configuration consisted of a light source, polarizer, sample, 50 kHz polarization modulator, and analyzer followed by a monochromator and detector or a multiwavelength detector. The light source was a xenon arc lamp with a spectral range from UV to near IR, i.e., a wavelength range of 190−2100 nm. In our experiments, the spectral range of 191 – 824 nm was selected, as this range was sufficient for the characterization of the film and gave a relatively fast acquisition time by using the multiwavelength mode (MWL). The angle of incidence was set to 70°. The beam diameter used in our experiments was 1.2 mm, yielding a spot size of 2.1 mm at the interface. The azimuth settings of modulator (M) and analyzer (A) were 0°and +45°, respectively. The data acquisition in the MWL mode was performed every three minutes for several hours. Since prolonged exposure to UV light

destabilized the film, wavelengths in the range of UV radiation were excluded from the beam by using an appropriate UV filter, when performing long (more than 10 hours) acquisitions.

Data modelling was done using a four-layer model, i.e., silicon, SiO_2, polystyrene, and lipid film layer. The film layer was assumed to be composed of lipids and water, whose percentages (assumed to be constant along the height of the film) were left as free fitting parameters for obtaining the resulting film thickness. The DeltaPsi2 modeling package (HORIBA Jobin Yvon) was applied to determine the film thickness and the optical properties of the interfacial film. For the theoretical model, software default values of the optical constants for the silicon, the SiO_2 and the polystyrene layers were used. The optical constants for the lipid layer were previously determined by refractometry and Cauchy's equation was applied to account for the wavelength dependence of the refractive index[35]. To fit the data and hence obtain the values of film thickness, the Lorentz oscillator model (slightly modified for better describing the lipid film properties) was used in all the measurements; due to the use of polystyrene, the fitted wavelength range was then limited to 451 – 800 nm. To minimize the mean-squared error of the fitting, the Levenberg−Marquardt algorithm was employed.

Atomic Force Microscopy

A 10 mg/ml GMO solution in chloroform was spin coated on ZYB grade Highly Oriented Pyrolytic Graphite (Bruker, USA). The sample was then inserted into the AFM fluid cell (filled with ultrapure water) and left equilibrating for two hours before starting the experiments.

AFM setup

AFM experiments were performed at room temperature on a Bruker Multimode 8 (equipped with Nanoscope V electronics, a sealed fluid cell and a type JV piezoelectric scanner) using Bruker SNL-A probes (triangular cantilever, nominal tip curvature radius 2–12 nm, nominal elastic constant 0.35 Nm^{-1}) calibrated with the thermal noise method[36]. The AFM fluid cell was then filled with ultrapure water.

Imaging

Imaging was performed in PeakForce mode. When scanning larger areas, the applied force setpoint was kept in the 150-250 pN range and lateral probe velocity was not allowed to exceed 5μm/s. This type of parameter optimization allowed for an accurate description of the film profile and estimation of its thickness. The average height value of all bare substrate zones was taken as the baseline zero height reference. Image background subtraction and thickness estimation were performed using Gwyddion 2.53[37]. For revealing the presence of the cubic architecture, 100x100 nm^2 areas of the sample were scanned. In this case, parameters like force setpoint, gain and lateral probe velocity were optimized in order to achieve the best image quality and hence resolve the cubic lattice. Both image analysis and calculation of the autocorrelation function (ACF) were performed in Gwyddion 2.53[37]. From the autocorrelation function image, it was then possible to obtain the profiles of the peaks and valleys defining the cubic architecture and hence to estimate the average lattice parameter of the whole structure (more details in the SI).

Force Spectroscopy

The mechanical response of the cubic phase lipid film was characterized by means of AFM-Force Spectroscopy. To this end, we recorded a series of force-distance curves at multiple XY positions (typically around 64-100 curves arranged in a square array) located on the surface of the lipid film. The acquired curves were then analyzed using a custom Python script automatically applying a Savitzky-Golay filter for noise smoothing, then discarding curves not presenting any indentation peak, finally locating each peak position within a curve. The procedure was iterated for all the recorded curves; a total of 211 curves were used for the analysis.

Results

In order to obtain $SQ_{II}^{D}Fs$ approaching the thicknesses of natural Q_{II} membranes, GMO was dissolved in chloroform at a concentration of 10 mg/ml and subsequently spin-coated on the different experimental substrates. As reported by Rittman et al.[19], this procedure yields an iridescent film that can be subsequently hydrated in order to allow the GMO molecules to self-assemble into the expected cubic architecture (Q_{II}^{D} phase for room temperature, atmospheric pressure and excess water); all these steps are graphically schematized in Figure 1.

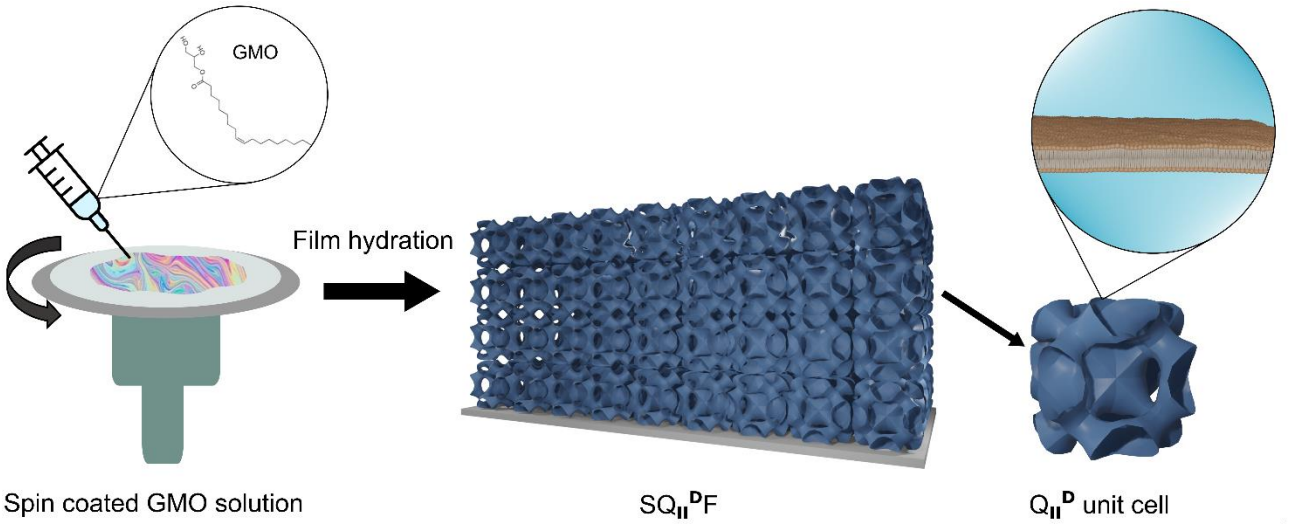

Figure 1: Fabrication of SQ$_{II}^{D}$Fs. The GMO/chloroform solution is deposited on top of a rigid substrate which is then put under rotation using a spin coater. This results in an iridescent film, visible to the naked eye, which can then be hydrated to allow GMO to self-assemble into the expected cubic architecture. At room temperature, atmospheric pressure and in excess of water, the resulting lipid film will be characterized by the repetition of multiple Q$_{II}^{D}$ (Pn-3m space group symmetry) unit cells in the 3D space, hence generating the so called Q$_{II}^{D}$ phase. The surface of each unit cell presents a lipid bilayer that cover the whole IPMS.

For SAXS, the GMO solution was directly spin-coated on the Kapton windows of the measuring cells; films were then hydrated and probed using X-rays (see Experimental section for more details). Figure 2 shows the diffractogram of the GMO-based lipid film prepared from a 10 mg/ml GMO:chloroform solution, compared with the ones obtained from more concentrated GMO:chloroform solutions (100 and 1000 mg/ml). For comparison, the diffractogram of the fully hydrated bulk phase (see the Experimental section for sample preparation) is also included. Despite forming a conspicuous, homogeneous iridescent film, after being spin-coated on the substrate from a 10 mg/ml GMO:chloroform solution, no Bragg peaks are visible in the diffractogram.

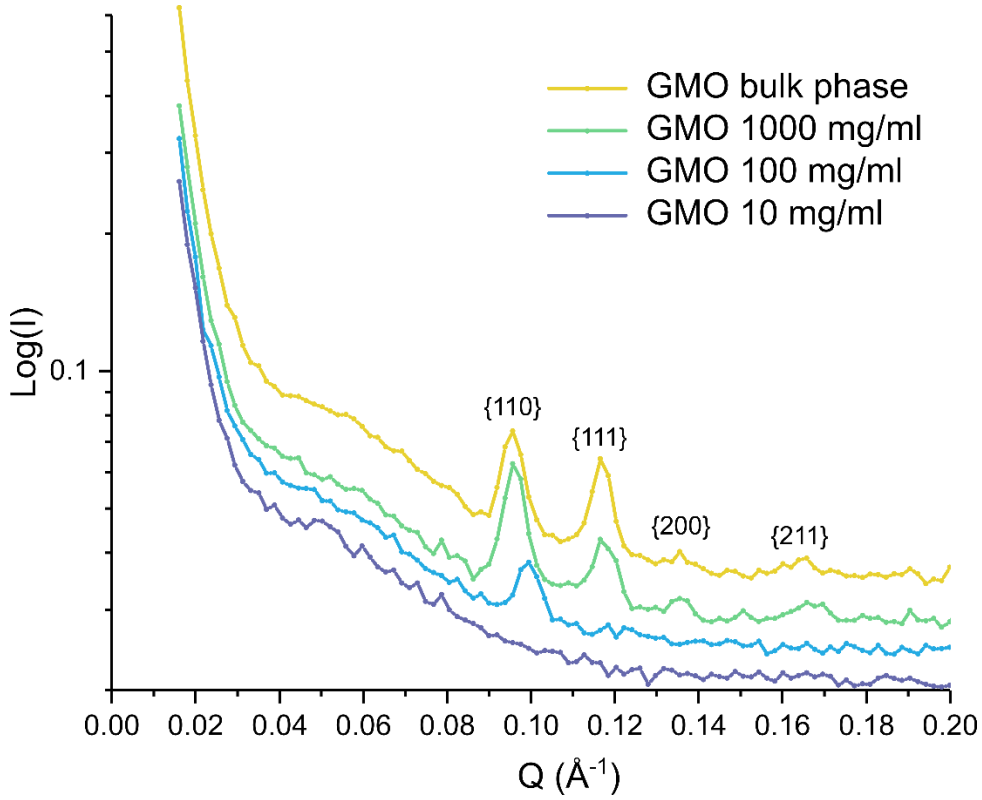

Figure 2: SAXS characterization of lipid Q_{II}^{D} phase films at different GMO concentrations. While it is not possible to identify any Bragg peak in the more diluted sample (purple curve), they become more pronounced as the concentration of the sample is increased (until reaching the bulk phase). Peak positions are compatible with the formation of an ordered Q_{II}^{D} phase, at all concentrations.

This is most likely due to the relatively low intensity of the x-ray source in the lab SAXS setup employed for the measurements, which does not allow resolving the diffraction pattern from the limited number of cubic domains in the obtained thin lipid film. However, using more concentrated GMO:chloroform solutions (which yield thicker films by spin coating) resulted in progressively more defined Bragg peaks.

The position of the single peak from the sample prepared from 100 mg/ml GMO:chloroform solution is compatible with the crystallographic plane identified by the {1 1 0} Miller indexes and corresponds to a lattice parameter of 90 Å while the lattice parameters determined for the film from a 1000 mg/ml GMO:chloroform solution and bulk phase are 92.6 ± 0.2 Å and 92.8 ± 0.3 Å, respectively (determined using the {1 1 0}, {1 1 1}, {2 0 0} and {2 1 1} Miller indexes, as described in Figure 2). The analysis of the Bragg peaks position is consistent with the formation of an ordered Q_{II}^{D} architecture that is mostly independent of the film thickness. All these results thus suggest that the same lipid arrangement should also be present in the sample obtained from the 10 mg/ml GMO:chloroform

solution, despite it not being detectable by our lab SAXS setup. Due to this, the 10 mg/ml sample was further investigated to confirm the formation of $SQ_{II}^{D}Fs$.

Ellipsometry was used to confirm the formation of a thin $SQ_{II}^{D}F$ from the 10 mg/ml GMO:chloroform solution; more precisely, to measure the thickness and the stability of the lipid film over time. Since Kapton cannot be probed by polarized visible light, the lipid solution was spin-coated on a silicon substrate coated with a thin polystyrene layer. As shown in Figure 3, Ellipsometry reveals the formation of a continuous lipid film with a thickness of 110-150 nm. Results from Figure 3 also reveal that the lipid film is destabilized by UV light, after an exposure of ~ 6 hours, while the film remains stable for more than 15 hours in visible light.

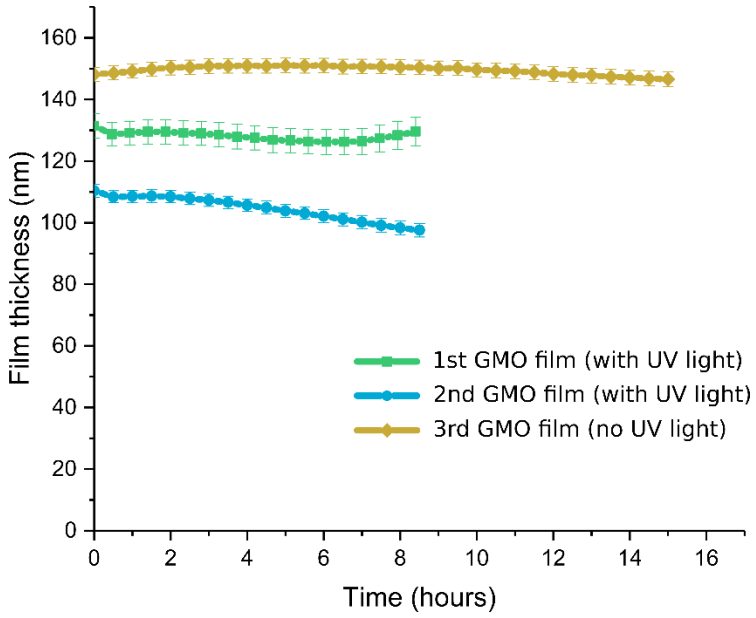

Figure 3: Results from the Ellipsometry analysis. Film thickness ranges from 110 to 150 nm. The 1st and 2nd acquisitions (green squares and blue circles) were performed using the entire wavelength spectrum (including UV light); as can be seen from the plot, after ~ 6 hours, the film is destabilized by prolonged exposures to UV light. The measurement without UV light (gold diamonds) shows that the lipid film remains stable and preserves its original thickness even after 15 hours.

Polystyrene is partially miscible with the chloroform contained in the GMO solutions and this might have introduced some contamination of the lipid film. The effect of a 10 µl droplet of chloroform on the polystyrene substrate was checked by ellipsometry and revealed an average 10 nm decrease in the layer thickness; this effect was considered during the fitting procedure for estimating the thickness of the GMO films. Nevertheless, since GMO is not miscible with polystyrene, this contamination would only pertain to the lowest layer, not significantly influencing the lipid film. Unfortunately, these ellipsometry measurements are not possible on the Kapton substrates, but

Kapton is known to have excellent resistance towards chloroform. There for the effect of Kapton solubilization is negligible and is not expected to influence the SAXS patterns, which is related to the whole lipid layer. The local surface structure of these thin lipid films was then determined via AFM imaging in liquid. Image analysis reveals that the probed lipid film presented a cubic architecture, directly exposed to the water interface (Figure 4a). According to Larsson [38], one of the two water channel networks must be capped at the surface of a bicontinuous cubic phase assembly, to ensure bilayer continuity. The pattern displayed in Figure 4 a and b therefore only represents the channel network open to the bulk water. This means that the observed features are separated by a distance equal to a\sqrt2, where a is the lattice parameter (for a more detailed representation and description refer to the work by Rittman et al. [19]). After performing routine image postprocessing procedures, the calculation of the 2D autocorrelation function (ACF)[37] (Figure 4b) allows reducing the background noise and estimating a lattice parameter of 97.6 ± 0.3 Å (please refer to the SI for further details about the calculation). This is in good agreement with the SAXS analysis performed on thicker films and compatible with a Q_{II}^{D} phase.

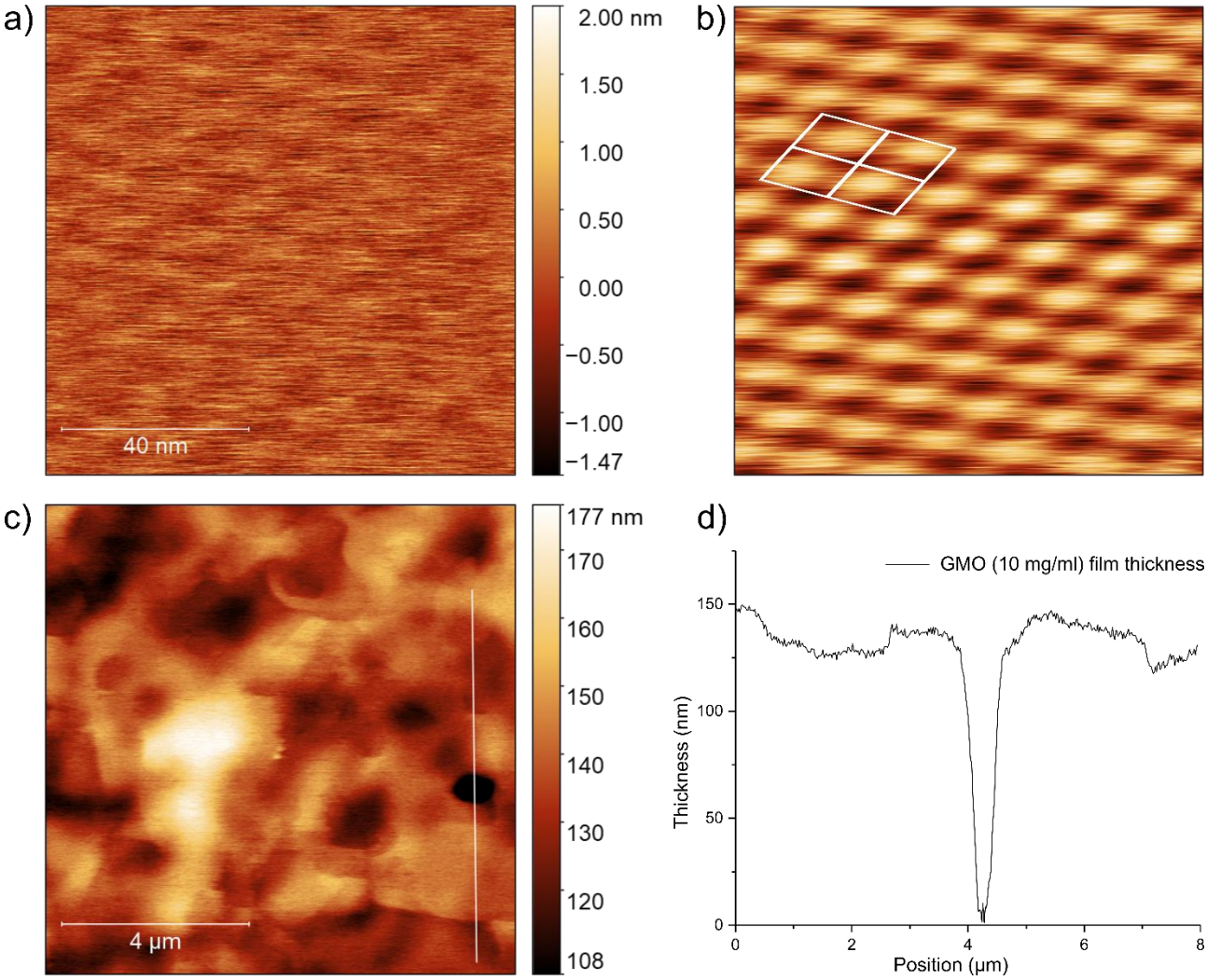

Figure 4: AFM imaging characterization of nanometric GMO-based lipid films: a) the topography of the film surface shows that the film possesses a cubic architecture, exposed to the water interface; b) applying a 2D ACF to the raw AFM image allows noise reduction and calculating the lattice parameter from the observed unit cell lattice pattern (white frame); c) 10x10 µm^2 topography of the lipid film, confirming the presence of an essentially continuous film; d) height profile along white line in panel c. Occasional $SQ_{II}^{D}F$ discontinuities allow estimating its thickness (≈150 nm).

Film morphology at larger length scales was then assessed by performing AFM imaging on 10x10 µm^2 regions (Figure 4c). As estimated via AFM images, film thickness was ~150 nm (Figure 4d), in agreement with ellipsometry results. The results are also consistent with those proposed by Rittman et al.[19], who determined a lattice parameter of 100 ± 10 Å for similar spin-coated cubic phase lipid films.

After characterizing their structure, $SQ_{II}^{D}Fs$ were employed as cubic membrane models for investigating the mechanics of these non-lamellar lipid architectures. To this purpose, AFM-FS was used for probing the mechanical response of the Q_{II}^{D} lipid architecture to nanoscale deformations.

In a typical AFM-FS experiment, the AFM tip is used to indent the sample and study its mechanical response to deformations (Figure 5). The forces experienced by the AFM tip while indenting the sample are recorded as a function of its penetration depth and plotted as force-distance curves (Figure 6a). The results from the AFM-FS measurements demonstrate that the mechanical response of the Q_{II}^{D} cubic architecture is completely different from the typical Hertzian regime observed for SLBs[39]. As exemplified by the force-distance curve shown in Figure 6a, after an initial, approximately linear regime, all the recorded force curves are characterized by a sequence of indentation peaks. Each peak corresponds to the sequential mechanical failure of successive cubic unit cells. Interestingly, the force required to penetrate each unit cell seems to be independent of the penetration depth, meaning that the mechanical resistance of each cubic unit is relatively unaffected by the ones located in lower regions of the film, which still have to be indented.

While the mechanical properties of these nanoarchitectures are still not fully understood at the nanoscale, IPMS-inspired macroscopic structures are gaining increasing attention in engineering applications where their combination of light weight, high impact- and stress-resistance represents a promising solution for multiple structural challenges[25–28].

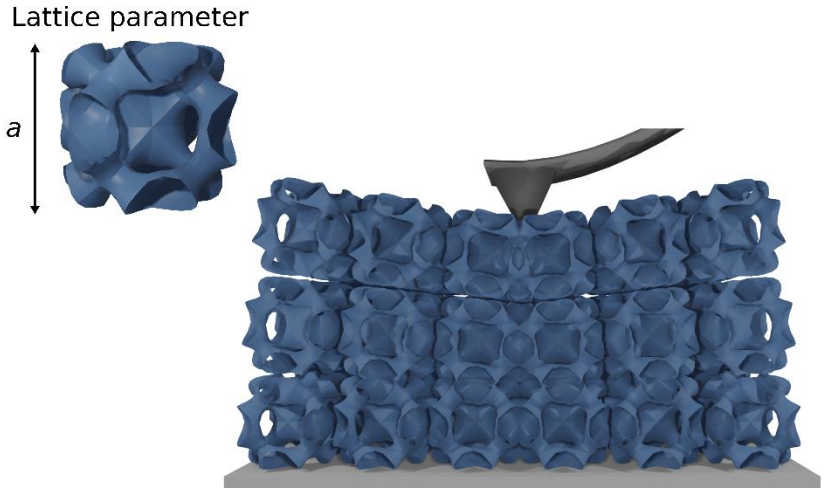

Figure 5: Representation of a typical AFM-FS experiment on a Q_{II}^{D} phase film; the AFM tip indents the sample causing a deflection of the cantilever. Recording the forces experienced during the indentation allows analyzing the mechanical response of the sample.

Even though these macroscopic structures and Q_{II} lipid membranes have vastly different length scales, they share the same topology. This suggests that some of the mechanical

properties studied on macroscopic Q_{II} structures could remain valid for their nanoscale counterparts and could help the development of potential bioinspired nanomaterials.

Comparing our AFM-FS curves with the ones obtained from compression tests on macroscopic 3D printed IPMS-inspired architectures[25,26,28] reveals the same peculiar mechanical response emerging in both samples, despite their length scales differing by more than six orders of magnitude. This observation suggests that the mechanical behaviour of these structures is mostly conserved even at the nanoscale.

The indentation peaks located along the force-distance curves can also be used to obtain a complementary structural characterization of the Q_{II}^{D} mesophase. As can be seen in Figure 5, the height of each cubic unit cell also represents the characteristic length scale of the whole architecture, i.e., its lattice parameter.

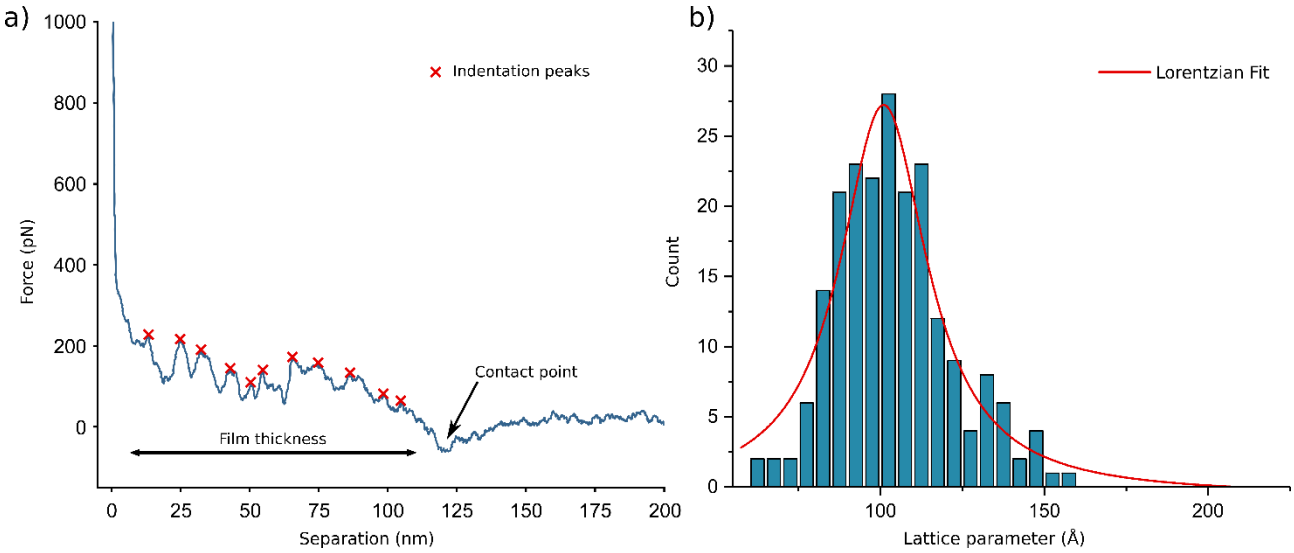

Figure 6: AFM-FS analysis of the lipid Q_{II}^{D} phase film: a) representative force-distance curve, describing the forces experienced by the AFM tip during the indentation of the cubic architecture; red crosses identify indentation peaks, corresponding to the mechanical failure of successive cubit unit cells; b) distribution of the lattice parameters obtained by dividing, in each force-distance curve, the value corresponding to the contact point by the number of peaks found in that specific curve; the distribution was fitted with a Lorentzian function and its centre was located at a lattice parameter value of ~100 Å, in agreement with previous SAXS and AFM imaging analyses.

It is possible to obtain this structural parameter from AFM-FS curves, by calculating, for each force-distance curve, the ratio between the observed film thickness (as determined by the contact point,

see Figure 6a) and the number of peaks found in that specific curve (i.e. the number of unit cells that were penetrated before reaching the substrate). Equation 1 summarizes the described procedure.

$$\frac{Film\ thickness}{n°\ of\ peaks\ (unit\ cells)} = Average\ lattice\ parameter \qquad (1)$$

This allows us to obtain a direct estimation of the vertical separation between successive cells. Estimates from 211 curves were then pooled, yielding a monomodal distribution of values (Figure 6b) which can be fitted with a Lorentzian function centered at ~100 Å, in agreement with the lattice parameters from both the SAXS and the AFM imaging analyses (92.6 Å and 97.6 Å, respectively). According to our knowledge, this analysis provides the first example in the literature on the use of AFM-FS for characterizing the structure of non-lamellar lipid membranes. Despite lacking the accuracy of the more traditional scattering (involving both X-rays and/or neutrons)[18,40,41] and cryo-electron microscopy[6,42] techniques, AFM-FS represents an alternative way to obtain a structural analysis of these lipid mesophases surface layers.

Conclusions

In conclusion, this work reports on the fabrication of thin supported lipid films with nanometric thickness, presenting a Q_{II}^{D} architecture. After probing the structure and the stability of the systems by means of SAXS, Ellipsometry and AFM imaging, AFM-FS was used to obtain the first nanomechanical characterization of these membranes. Differentiating from classical rheological studies, which could only provide bulk characterizations, AFM-FS allowed us to probe the mechanics of these lipid architectures via forces occurring at the nanoscale level and generating localized deformations, that resemble the ones involved in biological membrane interactions[32]. The mechanical response of the probed lipid Q_{II}^{D} phase films also revealed interesting analogies with studies performed on similar macroscopic 3D printed structures, suggesting that the response of these architectures to an applied force is independent of their size and related to their topology. This finding could help the development of bioinspired nanomaterials but also promote the use of macroscale membrane models for understanding the complex mechanics of these non-lamellar lipid architectures. Finally, AFM-FS was employed for estimating the lattice parameter of the probed Q_{II}^{D} membranes; the analysis of the force-distance curves gave results in good agreement with both the previous SAXS and AFM imaging experiments. In this context, our AFM-FS analysis provides the

first example of this technique being used for characterizing the structure of non-lamellar lipid mesophases, thus offering an alternative solution to the more commonly used scattering and cryo-electron microscopy-based techniques.

Acknowledgements

This research has received funding from the Horizon 2020 Framework Programme under the grants FETOPEN-801367 “evFOUNDRY” and FETPROACT-952183 "Biogenic Organotropic Wetsuits (BOW)”. We thank the SPM@ISMN research facility for support in the AFM experiments.

Bibliography

[1] R. Mezzenga, J.M. Seddon, C.J. Drummond, B.J. Boyd, G.E. Schröder-Turk, L. Sagalowicz, Nature-Inspired Design and Application of Lipidic Lyotropic Liquid Crystals, Adv. Mater. 31 (2019). https://doi.org/10.1002/adma.201900818.

[2] G.C. Shearman, O. Ces, R.H. Templer, J.M. Seddon, Inverse lyotropic phases of lipids and membrane curvature, J. Phys. Condens. Matter. 18 (2006). https://doi.org/10.1088/0953-8984/18/28/S01.

[3] K. Larsson, Cubic lipid-water phases: Structures and biomembrane aspects, J. Phys. Chem. 93 (1989) 7304–7314. https://doi.org/10.1021/j100358a010.

[4] J. Zhai, S. Sarkar, C.E. Conn, C.J. Drummond, Molecular engineering of super-swollen inverse bicontinuous cubic and sponge lipid phases for biomedical applications, Mol. Syst. Des. Eng. (2020). https://doi.org/10.1039/d0me00076k.

[5] Z.A. Almsherqi, T. Landh, S.D. Kohlwein, Y. Deng, Chapter 6 Cubic Membranes. The Missing Dimension of Cell Membrane Organization, Int. Rev. Cell Mol. Biol. (2009). https://doi.org/10.1016/S1937-6448(08)02006-6.

[6] D. Demurtas, P. Guichard, I. Martiel, R. Mezzenga, C. Hébert, L. Sagalowicz, Direct visualization of dispersed lipid bicontinuous cubic phases by cryo-electron tomography, Nat.

Commun. 6 (2015). https://doi.org/10.1038/ncomms9915.

[7] S. Andersson, S. Lidin, S.T. Hyde, K. Larsson, Minimal Surfaces and Structures: From Inorganic and Metal Crystals to Cell Membranes and Biopolymers, Chem. Rev. 88 (1988). https://doi.org/10.1021/cr00083a011.

[8] H.M.G. Barriga, M.N. Holme, M.M. Stevens, Cubosomes: The Next Generation of Smart Lipid Nanoparticles?, Angew. Chemie - Int. Ed. 58 (2019) 2958–2978. https://doi.org/10.1002/anie.201804067.

[9] T.G. Meikle, C.J. Drummond, F. Separovic, C.E. Conn, Membrane-mimetic inverse bicontinuous cubic phase systems for encapsulation of peptides and proteins, in: Adv. Biomembr. Lipid Self-Assembly, 2017. https://doi.org/10.1016/bs.abl.2017.01.002.

[10] M. Mendozza, L. Caselli, A. Salvatore, C. Montis, D. Berti, Nanoparticles and organized lipid assemblies: From interaction to design of hybrid soft devices, Soft Matter. 15 (2019) 8951–8970. https://doi.org/10.1039/c9sm01601e.

[11] V. Cherezov, H. Fersi, M. Caffrey, Crystallization screens: Compatibility with the lipidic cubic phase for in meso crystallization of membrane proteins, Biophys. J. 81 (2001) 225–242. https://doi.org/10.1016/S0006-3495(01)75694-9.

[12] V. Cherezov, J. Clogston, Y. Misquitta, W. Abdel-Gawad, M. Caffrey, Membrane protein crystallization in meso: Lipid type-tailoring of the cubic phase, Biophys. J. 83 (2002) 3393–3407. https://doi.org/10.1016/S0006-3495(02)75339-3.

[13] M. Caffrey, A comprehensive review of the lipid cubic phase or in meso method for crystallizing membrane and soluble proteins and complexes, Acta Crystallogr. Sect. FStructural Biol. Commun. 71 (2015) 3–18. https://doi.org/10.1107/S2053230X14026843.

[14] C. Montis, B. Castroflorio, M. Mendozza, A. Salvatore, D. Berti, P. Baglioni, Magnetocubosomes for the delivery and controlled release of therapeutics, J. Colloid Interface Sci. (2015). https://doi.org/10.1016/j.jcis.2014.11.056.

[15] M. Mendozza, C. Montis, L. Caselli, M. Wolf, P. Baglioni, D. Berti, On the thermotropic and magnetotropic phase behavior of lipid liquid crystals containing magnetic nanoparticles, Nanoscale. (2018). https://doi.org/10.1039/c7nr08478a.

[16] M. Fornasier, S. Biffi, B. Bortot, P. Macor, A. Manhart, F.R. Wurm, S. Murgia, Cubosomes stabilized by a polyphosphoester-analog of Pluronic F127 with reduced cytotoxicity, J. Colloid Interface Sci. (2020). https://doi.org/10.1016/j.jcis.2020.07.038.

[17] J. Gustafsson, H. Ljusberg-Wahren, M. Almgren, K. Larsson, Cubic Lipid−Water Phase Dispersed into Submicron Particles, Langmuir. 12 (1996). https://doi.org/10.1021/la960318y.

[18] A.P. Dabkowska, M. Valldeperas, C. Hirst, C. Montis, G.K. Pálsson, M. Wang, S. Nöjd, L. Gentile, J. Barauskas, N.J. Steinke, G.E. Schroeder-Turk, S. George, M.W.A. Skoda, T. Nylander, Non-Lamellar lipid assembly at interfaces: Controlling layer structure by responsive nanogel particles, Interface Focus. 7 (2017). https://doi.org/10.1098/rsfs.2016.0150.

[19] M. Rittman, M. Frischherz, F. Burgmann, P.G. Hartley, A. Squires, Direct visualisation of lipid bilayer cubic phases using Atomic Force Microscopy, Soft Matter. 6 (2010) 4058–4061. https://doi.org/10.1039/c002968h.

[20] M. Rittman, H. Amenitsch, M. Rappolt, B. Sartori, B.M.D. O'Driscoll, A.M. Squires, Control and analysis of oriented thin films of lipid inverse bicontinuous cubic phases using grazing incidence small-angle X-ray scattering, Langmuir. (2013). https://doi.org/10.1021/la401580y.

[21] A.M. Squires, J.E. Hallett, C.M. Beddoes, T.S. Plivelic, A.M. Seddon, Preparation of films of a highly aligned lipid cubic phase, Langmuir. (2013). https://doi.org/10.1021/la304726m.

[22] E.T. Castellana, P.S. Cremer, Solid supported lipid bilayers: From biophysical studies to sensor design, Surf. Sci. Rep. 61 (2006) 429–444. https://doi.org/10.1016/j.surfrep.2006.06.001.

[23] C. V. Kulkarni, W. Wachter, G. Iglesias-Salto, S. Engelskirchen, S. Ahualli, Monoolein: A magic lipid?, Phys. Chem. Chem. Phys. (2011). https://doi.org/10.1039/c0cp01539c.

[24] S.T. Hyde, S. Andersson, B. Ericsson, K. Larsson, A cubic structure consisting of a lipid bilayer forming an infinite periodic minimum surface of the gyroid type in the glycerolmonooleat-water system, Zeitschrift Fur Krist. - New Cryst. Struct. 168 (1984). https://doi.org/10.1524/zkri.1984.168.1-4.213.

[25] M.M. Sychov, L.A. Lebedev, S. V. Dyachenko, L.A. Nefedova, Mechanical properties of energy-absorbing structures with triply periodic minimal surface topology, Acta Astronaut. 150

(2018) 81–84. https://doi.org/10.1016/j.actaastro.2017.12.034.

[26] D.W. Abueidda, M. Bakir, R.K. Abu Al-Rub, J.S. Bergström, N.A. Sobh, I. Jasiuk, Mechanical properties of 3D printed polymeric cellular materials with triply periodic minimal surface architectures, Mater. Des. 122 (2017) 255–267. https://doi.org/10.1016/j.matdes.2017.03.018.

[27] L. Zhang, S. Feih, S. Daynes, S. Chang, M.Y. Wang, J. Wei, W.F. Lu, Energy absorption characteristics of metallic triply periodic minimal surface sheet structures under compressive loading, Addit. Manuf. 23 (2018) 505–515. https://doi.org/10.1016/j.addma.2018.08.007.

[28] Z. Qin, G.S. Jung, M.J. Kang, M.J. Buehler, The mechanics and design of a lightweight three-dimensional graphene assembly, Sci. Adv. 3 (2017). https://doi.org/10.1126/sciadv.1601536.

[29] C. Rodríguez-Abreu, M. García-Roman, H. Kunieda, Rheology and dynamics of micellar cubic phases and related emulsions, Langmuir. 20 (2004) 5235–5240. https://doi.org/10.1021/la0498962.

[30] R. Mezzenga, C. Meyer, C. Servais, A.I. Romoscanu, L. Sagalowicz, R.C. Hayward, Shear rheology of lyotropic liquid crystals: A case study, Langmuir. 21 (2005) 3322–3333. https://doi.org/10.1021/la046964b.

[31] C. Speziale, R. Ghanbari, R. Mezzenga, Rheology of Ultraswollen Bicontinuous Lipidic Cubic Phases, Langmuir. 34 (2018) 5052–5059. https://doi.org/10.1021/acs.langmuir.8b00737.

[32] G. Bao, S. Suresh, Cell and molecular mechanics of biological materials, Nat. Mater. 2 (2003) 715–725. https://doi.org/10.1038/nmat1001.

[33] M. Mendozza, C. Montis, L. Caselli, M. Wolf, P. Baglioni, D. Berti, On the thermotropic and magnetotropic phase behavior of lipid liquid crystals containing magnetic nanoparticles, Nanoscale. 10 (2018) 3480–3488. https://doi.org/10.1039/c7nr08478a.

[34] S. Murgia, F. Caboi, M. Monduzzi, H. Ljusberg-Wahren, T. Nylander, Acyl migration and hydrolysis in monoolein-based systems, in: T. Nylander, B. Lindman (Eds.), Prog. Colloid Polym. Sci., Springer Berlin Heidelberg, Berlin, Heidelberg, 2002: pp. 41–46. https://doi.org/10.1007/3-540-45291-5_6.

[35] A. Stamm, A. Svendsen, J. Skjold-Jørgensen, T. Vissing, I. Berts, T. Nylander, The

triolein/aqueous interface and lipase activity studied by spectroscopic ellipsometry and coarse grained simulations, Chem. Phys. Lipids. 211 (2018) 37–43. https://doi.org/10.1016/j.chemphyslip.2017.10.011.

[36] J.L. Hutter, J. Bechhoefer, Calibration of atomic-force microscope tips, Rev. Sci. Instrum. 64 (1993) 1868–1873. https://doi.org/10.1063/1.1143970.

[37] D. Nečas, P. Klapetek, Gwyddion: An open-source software for SPM data analysis, Cent. Eur. J. Phys. 10 (2012) 181–188. https://doi.org/10.2478/s11534-011-0096-2.

[38] K. Larsson, Aqueous dispersions of cubic lipid–water phases, Curr. Opin. Colloid Interface Sci. 5 (2000) 64–69. https://doi.org/https://doi.org/10.1016/S1359-0294(00)00040-6.

[39] S. Garcia-Manyes, F. Sanz, Nanomechanics of lipid bilayers by force spectroscopy with AFM: A perspective, Biochim. Biophys. Acta - Biomembr. 1798 (2010) 741–749. https://doi.org/10.1016/j.bbamem.2009.12.019.

[40] P. Garstecki, R. HoŁyst, Scattering patterns of self-assembled cubic phases: 2. Analysis of the experimental spectra, Langmuir. 18 (2002) 2529–2537. https://doi.org/10.1021/la011299h.

[41] B. Angelov, A. Angelova, V.M. Garamus, G. Lebas, S. Lesieur, M. Ollivon, S.S. Funari, R. Willumeit, P. Couvreur, Small-angle neutron and X-ray scattering from amphiphilic stimuli-responsive diamond-type bicontinuous cubic phase, J. Am. Chem. Soc. 129 (2007) 13474–13479. https://doi.org/10.1021/ja072725+.

[42] S.B. Rizwan, Y.D. Dong, B.J. Boyd, T. Rades, S. Hook, Characterisation of bicontinuous cubic liquid crystalline systems of phytantriol and water using cryo field emission scanning electron microscopy (cryo FESEM), Micron. 38 (2007) 478–485. https://doi.org/10.1016/j.micron.2006.08.003.